Eurasian Subarctic Summer Climate in Response to Anomalous Snow Cover

SHINJI MATSUMURA AND KOJI YAMAZAKI

Faculty of Environmental Earth Science, Hokkaido University, Sapporo, Japan

(Manuscript received 6 October 2010, in final form 28 July 2011)

ABSTRACT

The summer climate in northern Eurasia is examined as a function of anomalous snow cover and processes associated with land–atmosphere coupling, based on a composite analysis using observational and reanalysis data. The analysis confirms that the snow–hydrological effect, which is enhanced soil moisture persisting later into the summer and contributing to cooling and precipitation recycling, is active in eastern Siberia and contributes to the formation of the subpolar jet through the thermal wind relationship in early snowmelt years.

Strong anticyclonic differences (early − late snowmelt years) with a baroclinic structure form over eastern Siberia as a result of surface heating through the snow–hydrological effect in early snowmelt years. Surface heating contributes to the development of thermally generated stationary Rossby waves that propagate eastward to eastern Siberia. Rossby wave activity is maintained into early autumn, together with cyclonic differences over far eastern Siberia, in conjunction with the early appearance of snow cover in this region. The anticyclonic differences over eastern Siberia act like a blocking anticyclone, thereby strengthening upstream storm track activity. Furthermore, it is possible that surface anticyclonic differences over the Arctic contribute to year-to-year variability of summer Arctic sea ice concentration along the Siberian coast. The results suggest that variations in northern Eurasian snow cover and associated land–atmosphere coupling processes have important implications for the predictability of Eurasian subarctic summer climate.

1. Introduction

The climate system of northern latitudes is a dynamic and interactive system involving couplings between atmospheric, oceanic, and land surface processes. Arctic and subarctic climate systems develop in response to a variety of meteorological conditions, related to both snow and ice. Snow cover and the presence of sea ice are two factors that impact climate and exhibit interannual temporal and spatial variations. Summer sea ice cover in the Arctic Ocean has experienced an accelerated decline during the past 10 years (e.g., Comiso et al. 2008). Similarly, the duration of snow cover in northern Eurasia has generally decreased over the past 40 years, due to a systematic retreat of late-spring snow cover (Groisman et al. 2006).

Figure 1 shows the distribution of snow and sea ice cover in June and July, in terms of the mean number of days with snow cover, and the sea ice concentration. Land areas in the Siberian subarctic are snow free by July, whereas ocean areas remain covered by sea ice in both June and July. This differential melting of snow and sea ice cover, caused by the early melting of land snow, results in a strong temperature gradient across the Arctic coastline. In autumn, far eastern Siberia is the first region in northern Eurasia to become covered by snow (see Fig. 13a). Eurasian snow variations also force the wintertime Arctic Oscillation (AO)-type variability (e.g., Watanabe and Nitta 1998; Cohen and Entekhabi 1999). Thus, cryospheric variations influence the surface heat budget (by introducing differential variations in the surface albedo of snow and sea ice) and introduce forcings that can amplify climate change and variability.

Far eastern Siberia is one region in the Northern Hemisphere where frequent blocking events occur (e.g., Tibaldi et al. 1994). These blocking events are associated with the cold regions of the Sea of Okhotsk, bounded to the north (far eastern Siberia) and west (eastern Siberia) by warm summertime landmasses. From late April to early September a quasi-stationary surface high pressure system often resides over the cold surface of the Sea of Okhotsk for several days or a week. The Okhotsk high is accompanied by blocking anticyclones in the upper troposphere over far eastern Siberia (e.g.,

Corresponding author address: Shinji Matsumura, Faculty of Environmental Earth Science, Hokkaido University, Sapporo 060-0810, Japan.
E-mail: matsusnj@ees.hokudai.ac.jp

DOI: 10.1175/2011JCLI4116.1

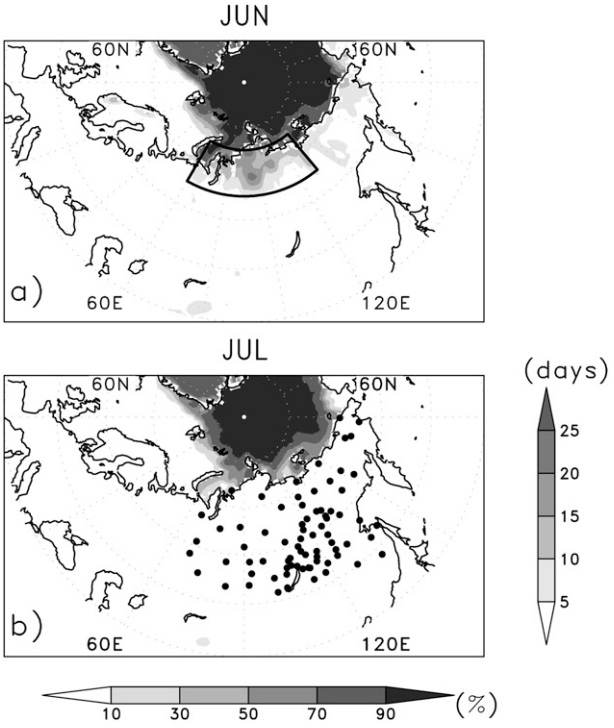

FIG. 1. Mean number of days with snow cover on land areas, as observed by SSM/I, and Arctic sea ice concentration (%) for the period 1988–2004 in (a) June and (b) July. The northern snow cover index was calculated for the bounded region in (a), and black solid circles in (b) indicate the locations of observation stations used in this study.

Ninomiya and Mizuno 1985a). The frequent occurrence of the Okhotsk high in July and August leads to abnormally cool summers due to the cool and wet surface northeasterlies in East Asia (e.g., Ninomiya and Mizuno 1985a,b). While the Okhotsk high has been regarded as one of the critical factors for seasonal forecasts of summertime weather in Japan, its skill remains to be developed, possibly resulting from complex interactions between the atmosphere, oceans, and land surfaces.

Snow has two main effects on climate (e.g., Barnett et al. 1989; Yasunari et al. 1991): the albedo effect, which is higher albedo leading to surface cooling, and the snow–hydrological effect, which is enhanced soil moisture persisting later into the summer, thus contributing to cooling and a coupling between evaporation and precipitation. It is generally easy to identify regions influenced by the albedo effect, as it requires snow cover. However, it is difficult to identify regions influenced by the snow–hydrological effect because this effect appears after snowmelt as climate memory. Matsumura et al. (2010b, hereafter MYT) examined the effect of anomalous springtime snow cover in northern Eurasia on the summertime land–atmosphere climate system using an atmospheric general circulation model (AGCM). In western Siberia, the albedo effect of snow has a significant influence on the surface heating and cooling. In eastern Siberia, the snow–hydrological effect is prominent during summertime, contributing to westerly anomalies in the light snow run. Furthermore, the subpolar jet is strengthened and maintained along the Arctic coast in early summer, causing Rossby wave activity to propagate eastward over northern Eurasia. MYT found that variations in springtime Eurasian snow cover are related to changes in summertime northern atmospheric and hydrologic circulation through land–atmosphere interactions.

The MYT sensitivity experiments are prescribed climatological sea surface temperature (SST) and sea ice boundary conditions, and do not consider processes related to soil freezing. We must therefore confirm the results of MYT, using both ground observations and reanalysis data. The present study incorporates these neglected processes by focusing on interannual variations in the snow cover and the resulting effects on the northern land–atmosphere climate system. We seek to understand interannual variations in the Arctic/subarctic climate system in terms of coupling among the atmosphere, land surface, and ocean.

The remainder of this paper is organized as follows. Section 2 describes the data and methods, and section 3 presents the snow–hydrological effect in eastern Siberia. Section 4 describes the dynamical responses of atmospheric circulation, including a comparison with the results presented by MYT. Section 5 discusses the influence of the responses on Arctic sea ice variability. Finally, a discussion of the results and the main conclusions are given in section 6.

2. Data and methods

Data for this study were acquired from the Baseline Meteorological Data in Siberia (BMDS) dataset (version 4.1), compiled and quality checked by the Global Energy and Water Cycle Experiment (GEWEX) Asian Monsoon Experiment (GAME)-Siberia project (Suzuki et al. 2009). The dataset contains daily mean data for 16 meteorological variables over a 19-yr period (1986–2004). We used the monthly means of soil surface and surface air temperature, and the daily minimum and maximum of surface air temperature, vapor pressure deficit, precipitation, snow coverage ratio, and snow depth obtained at 74 stations (Fig. 1b). Using this dataset, Park et al. (2008) reported the seasonal temporal and spatial characteristics of surface conditions in eastern Siberia. We also used the National Centers for Environmental

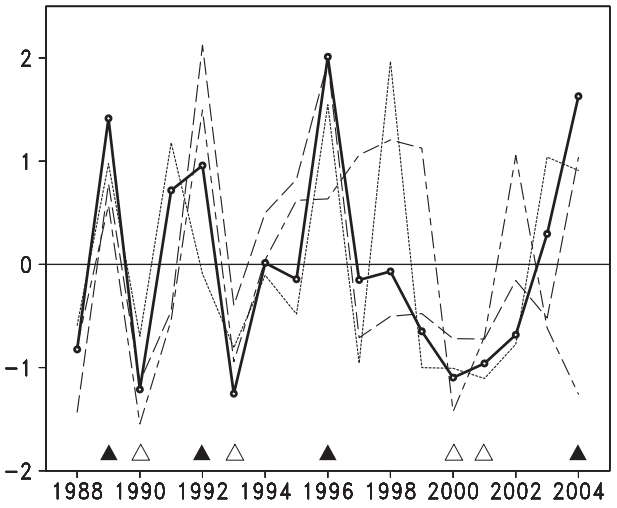

FIG. 2. Time series of the number of mean days with snow cover (normalized) observed by SSM/I (thick solid line) and at individual stations (thin lines) within the area averaged by 65°–75°N, 60°–130°E in June (see Fig. 1a). Black solid (open) triangles indicate LSY (ESY).

Prediction–Department of Energy Atmospheric Model Intercomparison Project reanalysis (R-2) (Kanamitsu et al. 2002), the Climate Prediction Center Merged Analysis of Precipitation (CMAP) (Xie and Arkin 1996), and the number of days with snow cover [measured with a Special Sensor Microwave Imager (SSM/I)] from the Japan Meteorological Agency (JMA 2005), and sea ice data from the Met Office Hadley Centre Sea Ice and Sea Surface Temperature version 1 (HadISST1) (Rayner et al. 2003).

We performed a composite analysis defined by a northern snow cover index (Fig. 1a) for the area bounded by 65°–75°N, 60°–130°E in June. The snow cover index indicates the normalized number of mean days with snow cover in June (Fig. 2) and reveals early-snowmelt years (ESY) (1990, 1993, 2000, 2001) and late-snowmelt years (LSY) (1989, 1992, 1996, 2004). We confirmed that the snow cover index reasonably corresponds to the leading empirical orthogonal function (EOF) mode of northern snow cover in June (EOF 1: 42.6%) and that snow cover anomalies correspond to snow depth anomalies over northern Eurasia (based on data from observation stations). The present study focuses on the approximately last 20 years; of course, the snow cover data has a decreasing trend (Fig. 2, the removed linear trend). In our analysis period (1988–2004), the interannual variations in the snow cover index indicate that the timing of snowmelt (early or late) is roughly consistent over the entirety of northern Eurasia, although the seasonal timing varies from March to June depending on the region (Shinoda et al. 2001). We confirmed that the snow cover index well reflects ESY and LSY in both SSM/I and station data (not shown). In this paper, using a similar method to MYT, we focus on ESY and discuss the ESY − LSY difference.

The snow–hydrological effect depends primarily on snow mass and soil moisture; however, systematic data on soil moisture in Siberia are not available for the period of this study. Consequently, as a proxy for soil moisture, we used soil surface and surface air temperature, and precipitation or vapor pressure deficit (the difference between the saturation vapor pressure and the actual vapor pressure); these parameters represent conditions at the land surface and in the near-surface atmosphere.

3. Snow–hydrological effect in eastern Siberia

Figure 3 shows distribution maps of composite analysis representing the ESY − LSY difference for June–August (JJA) mean values. Strong positive differences in the surface air temperature T_{sfc} are seen in western Siberia (the Yenisey Basin) and eastern Siberia (the Lena Basin), representing anomalous snow cover in these regions (Fig. 3a). As discussed by MYT, since snow covers northwestern Siberia until June (Fig. 1), a weakening of the albedo effect contributes to surface heating in ESY.

In the Lena Basin, the sensible heat flux in spring is higher than latent heat flux, while in summer, the latent heat flux is higher than sensible heat flux (Park et al. 2008), suggesting that the surface moisture conditions can affect T_{sfc} variability via the sensible heat flux in early summer. Decreased precipitation differences also occur over the Lena Basin (Fig. 3b; see also MYT) and correspond well to drier soil moisture differences when analyzing NCEP reanalysis in the surface soil layer (not shown). Since the local evaporation contributes much to the local precipitation in eastern Siberia (i.e., recycled water) (e.g., Numaguti 1999; Kurita et al. 2004), these results suggest that decreased snow cover (higher T_{sfc}) during the snowmelt period results in less snowmelt and correspondingly lower soil moisture in summer (higher T_{sfc}), resulting in turn in reduced evaporation and precipitation (MYT). Thus, these indicate that the snow–hydrological effect is active in eastern Siberia.

Positive differences in the water vapor deficit are seen in the Lena Basin (Fig. 3c). It is an indication of the drying potential of air and of potential evaporation (see also, e.g., Delworth and Manabe 1989). It is expected that the potential evaporation also increases in the Lena Basin. The difference between daily T_{sfc} maxima and minima increases in the Lena Basin (not shown), and variations in the diurnal T_{sfc} range are closely related to

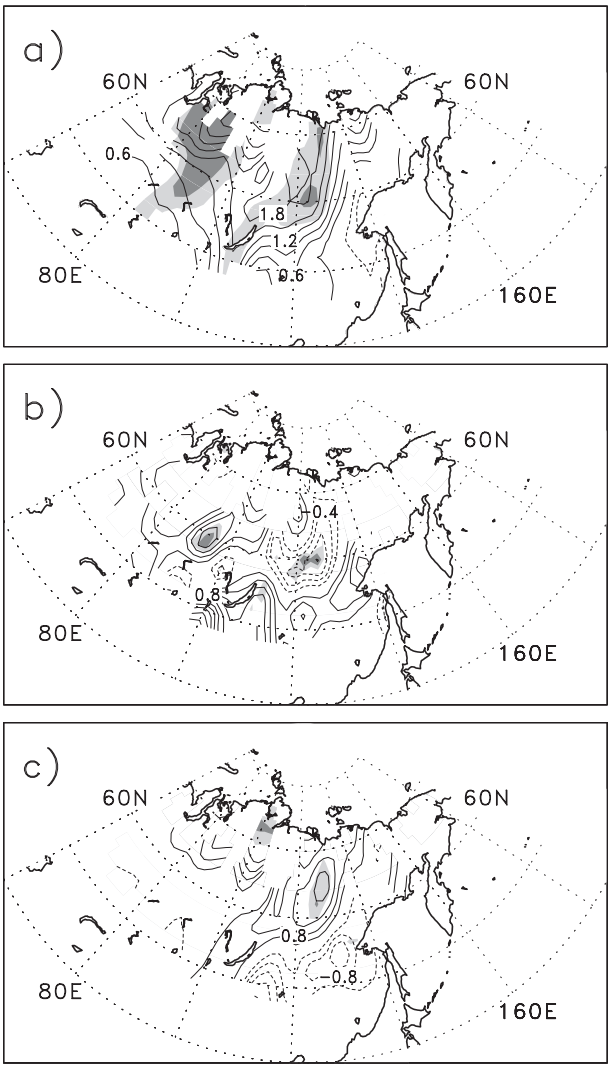

FIG. 3. Distribution maps of ESY − LSY difference for JJA means of (a) surface air temperature, (b) precipitation, and (c) vapor pressure deficit. Light (dark) shadings represent differences significant at the 90% (95%) confidence levels. Contour intervals are (a) 0.3°C, (b) 0.2 mm day^{-1}, and (c) 0.4 hPa (zero contours omitted).

variations in soil moisture and precipitation (Dai et al. 1999). Because surface air temperatures, as well as daily T_{sfc} maxima and minima, are high in the Lena Basin, the saturation of water vapor is suppressed in the atmospheric boundary layer. Consequently, we surmise that precipitation decreases over the Lena Basin during ESY.

We can confirm that the snow–hydrological effect contributes to summertime climate variations in eastern Siberia. Surface air temperature variability is sensitive to soil moisture conditions after snowmelt; because of dry ground conditions in eastern compared with western Siberia (MYT), snowmelt water effectively infiltrates the soils in this region. In addition, dry atmospheric conditions in eastern Siberia, where water vapor can sufficiently hold in the air, appear to contribute to precipitation variability. The combination of the snow–hydrological effect and coupling between evaporation and precipitation appears to maintain the surface heating or cooling in eastern Siberia.

4. Atmospheric circulation responses

The response of the atmospheric circulation to the snow–hydrological effect is focused on the months of July–September. We compare our result to the model proposed by MYT (but note that their model is based on the months of May–August).

a. Occurrence of the subpolar jet

Strong T_{sfc} variability affects the upper-tropospheric westerlies through the thermal wind relationship. Figure 4 (left panels) shows the monthly meridional 850-hPa temperature gradient ($-\partial T/\partial y$) differences. The temperature gradient differences increase along the Arctic coast in July (shadings and solid contours) and decrease in August. Strong positive differences over eastern Siberia in August correspond to enhanced T_{sfc} differences (Fig. 3a); the positive differences extend eastward, similar to the result of MYT. Figure 4 (right panels) shows the monthly 300-hPa zonal wind in ESY (solid contours) and the wind differences between ESY and LSY (shadings). Zonal wind patterns indicate that a subpolar jet forms along the Arctic coast in July and over eastern Siberia in August, forming a double-jet structure with the subtropical jet. The westerly differences corresponding to the subpolar jet are also enhanced over eastern Siberia and extend eastward in August. These increased westerlies correspond to strong temperature gradient differences.

Surface air temperatures in northern Siberia reach a maximum in July (e.g., Fig. 2 in MYT); the T_{sfc} gradient across the Arctic coast also reaches a maximum at this time because of low T_{sfc} values associated with sea ice in the Arctic Ocean (Fig. 1). In August, T_{sfc} begins to decrease and the land–sea contrast weakens slightly. As a result, the subpolar jet appears along the Arctic coast in July, while in August it appears over eastern Siberia. These results suggest that westerly differences corresponding to the subpolar jet are caused by the land–sea T_{sfc} contrast across the Arctic coast in July and by the snow–hydrological effect in eastern Siberia in August; these findings are consistent with the MYT model.

b. Development of a quasi-stationary Rossby wave

Stationary Rossby waves propagate along the subtropical jet as a waveguide (e.g., Hoskins and Ambrizzi

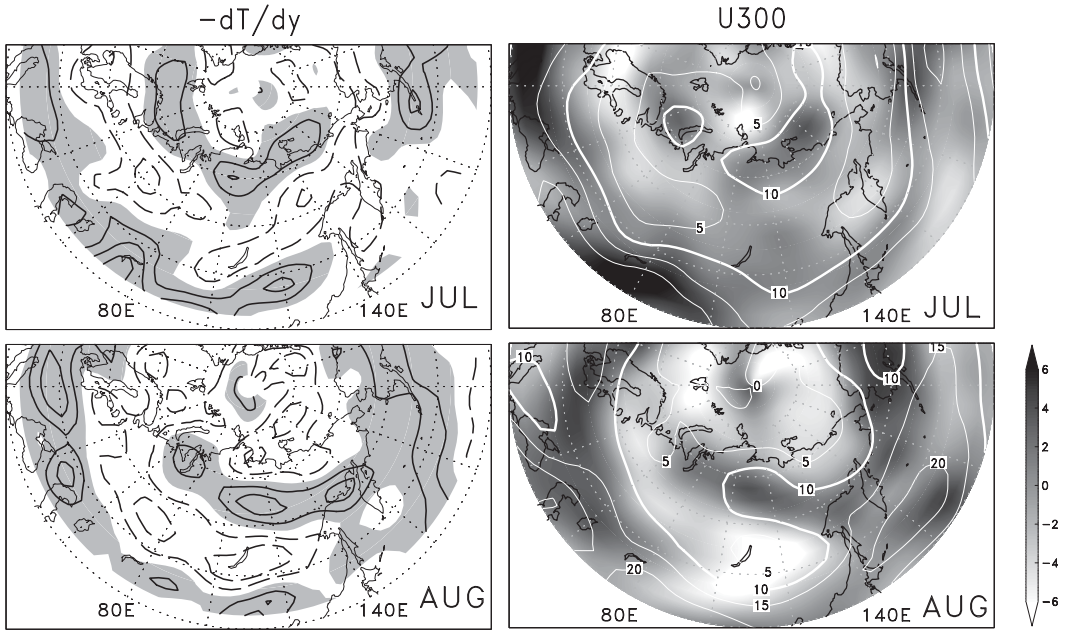

FIG. 4. (left) Monthly meridional 850-hPa temperature gradient ($-\partial T/\partial y$) differences (ESY − LSY) in July and August. Contour interval is 1×10^{-3} K km^{-1}, zero contour omitted; solid contours and shaded area represent positive values; dashed contours represent negative values. (right) Monthly 300-hPa zonal wind (m s^{-1}) in ESY (5 m s^{-1} contour interval) and the ESY − LSY difference (shaded). Thick solid contours indicate 10 m s^{-1}.

1993). For example, in late summer the localized descent over the eastern Mediterranean and Aral Seas coincides with the entrance region of the Asian jet and acts as stationary wave forcing (Enomoto et al. 2003). Similarly, in early summer the subpolar jet along the Arctic coast acts as a stationary Rossby waveguide (Nakamura and Fukamachi 2004; MYT). In this section, we discuss the development of a quasi-stationary Rossby wave along the subpolar jet as a result of the snow–hydrological effect in eastern Siberia.

Figure 5 shows monthly 300-hPa geopotential height differences and associated wave activity fluxes as defined by Takaya and Nakamura (2001). Anticyclonic differences over the Arctic are maintained in July and August. In July wave activity propagates eastward along the Arctic coast in the form of stationary Rossby wave packets. The Rossby waves appear to contribute to the formation of an upper-level ridge over far eastern Siberia. The enhanced westerlies form a subpolar jet, and the wave activity that accompanies the subpolar jet is enhanced by the land–sea temperature contrast across the Arctic coast; MYT reported similar findings. In August strong anticyclonic differences form over eastern Siberia, and a ridge extends southeastward toward northern Japan. A quasi-stationary Rossby wave is excited around eastern Siberia and propagates eastward over the Sea of Okhotsk; this wave activity is faintly visible in the MYT model. The enhanced westerlies form a subpolar jet over eastern Siberia, and the Rossby wave activity that accompanies the subpolar jet is also enhanced in this area.

To examine the source of the quasi-stationary Rossby wave in eastern Siberia, we show vertical cross sections of atmospheric parameters in August along 60°N (Figs. 6 and 7). Significant geopotential height differences (shadings) slope westward with height (Fig. 6a), reflecting the baroclinic structure in the troposphere. The lower-tropospheric response in eastern Siberia favors upward propagation of wave activity, and the longitudinal component in the upper troposphere is dominantly toward downstream areas, indicating that the stationary Rossby wave emanates from lower-tropospheric levels in eastern Siberia. Significant positive air temperature differences occur between the surface and the near tropopause (approximately 250 hPa) over eastern Siberia, while above the tropopause, air temperature differences are significantly negative (Fig. 6b).

In ESY, eastern Siberia at about 110°E is mainly a region of ascending air masses between the surface and upper troposphere (Fig. 7a); vertical velocity differences are also enhanced. The ascent occurs in conjunction with near-surface airmass convergence and upper-tropospheric divergence (Fig. 7b). The divergence acts as a forcing factor contributing to relative vorticity. Negative vorticities are located near the subpolar jet entrance over eastern Siberia (Fig. 7c), and these vorticity

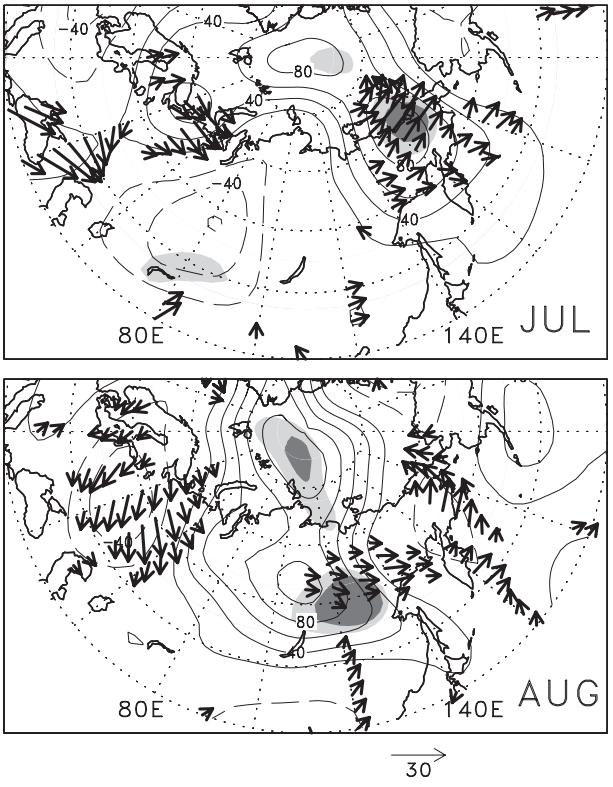

FIG. 5. Monthly 300-hPa geopotential height (20-m contour interval) differences (ESY − LSY) and associated wave activity fluxes ($m^2\ s^{-2}$) (arrows), as defined by Takaya and Nakamura (2001), in July and August. Light (dark) shadings represent differences significant at the 90% (95%) confidence level.

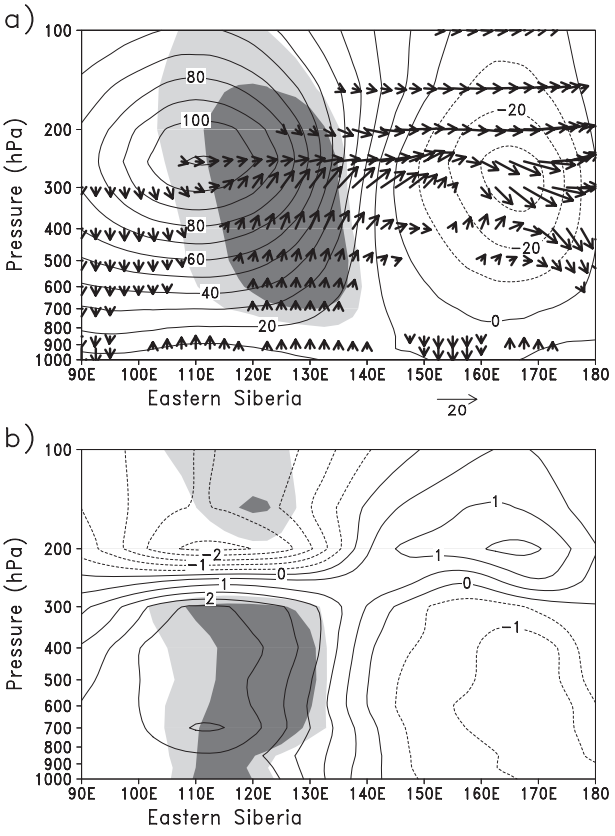

FIG. 6. Vertical cross sections of the ESY − LSY difference of (a) geopotential height (10-m contour interval) and (b) air temperature (0.5-K contour interval) along 60°N in August. Superimposed arrows indicate the longitude–vertical component of the wave activity flux ($m^2\ s^{-2}$). Light (dark) shadings represent differences significant at the 90% (95%) confidence level.

forcings are transported eastward by the propagation of quasi-stationary Rossby waves along the subpolar jet. The aforementioned results suggest that a stationary Rossby wave is thermally generated by anomalous surface heating as a consequence of the snow–hydrological effect. Descending air masses to the east of the ascent also occur in conjunction with upper-tropospheric convergence and near-surface divergence (Fig. 7b), resulting in surface anticyclonic differences in this area (Fig. 6a).

To further examine the tropospheric heating over eastern Siberia, we estimate the diagnostic heat budget, based on 6-hourly data interpolated at 25-hPa intervals, according to

$$\frac{\partial\theta}{\partial t} + u\frac{\partial\theta}{\partial x} + v\frac{\partial\theta}{\partial y} + \omega\frac{\partial\theta}{\partial p} = Q, \qquad (1)$$

where θ is the potential temperature, u is the zonal wind, v the meridional wind, ω the vertical velocity, and Q is the diabatic heating rate. Figure 8 shows the vertical and horizontal temperature advection and diabatic heating (residual heat) differences in the troposphere. Over eastern Siberia at about 110°E, the mid- and upper troposphere is affected by diabatic heating, caused by condensation heating, as a result of adiabatic cooling of ascending air masses. On the other hand, over eastern Siberia at about 130°E adiabatic heating caused by descending air masses contributes to mid- and upper-tropospheric heating and is compensated by diabatic cooling. Lower-tropospheric warm advection over the near-surface convergence at about 110°E is compensated by diabatic cooling. The lower troposphere between 120° and 130°E is affected by diabatic heating, which is compensated by cool advection, possibly a consequence of sensible heat transport due to surface heating. These results indicate that tropospheric heating is mainly caused by diabatic heating (condensation heating) associated with ascending air masses and adiabatic heating of descending air masses, as a result of ascending air masses due to surface heating through the snow–hydrological effect, forming strong anticyclonic differences with a baroclinic structure.

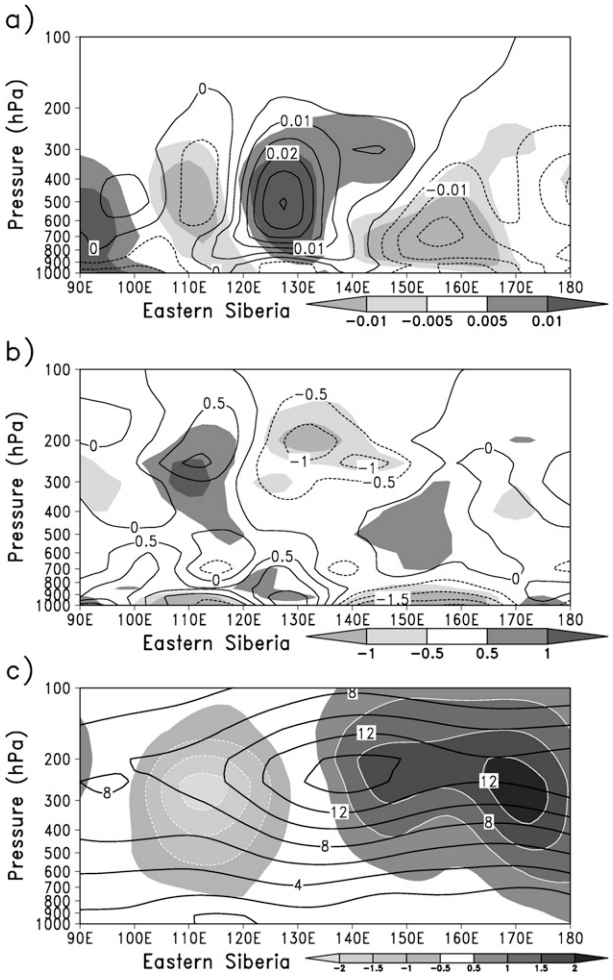

FIG. 7. As in Fig. 6, but for (a) vertical velocity (omega) (0.005 Pa s^{-1} contour interval; positive values downward) in ESY (contours) and ESY − LSY difference (shaded), (b) divergence (10^{-6} s^{-1}) in ESY (contours) and ESY − LSY difference (shaded), and (c) relative vorticity (shaded, 10^{-5} s^{-1}) and westerly wind (contours, m s^{-1}) in ESY.

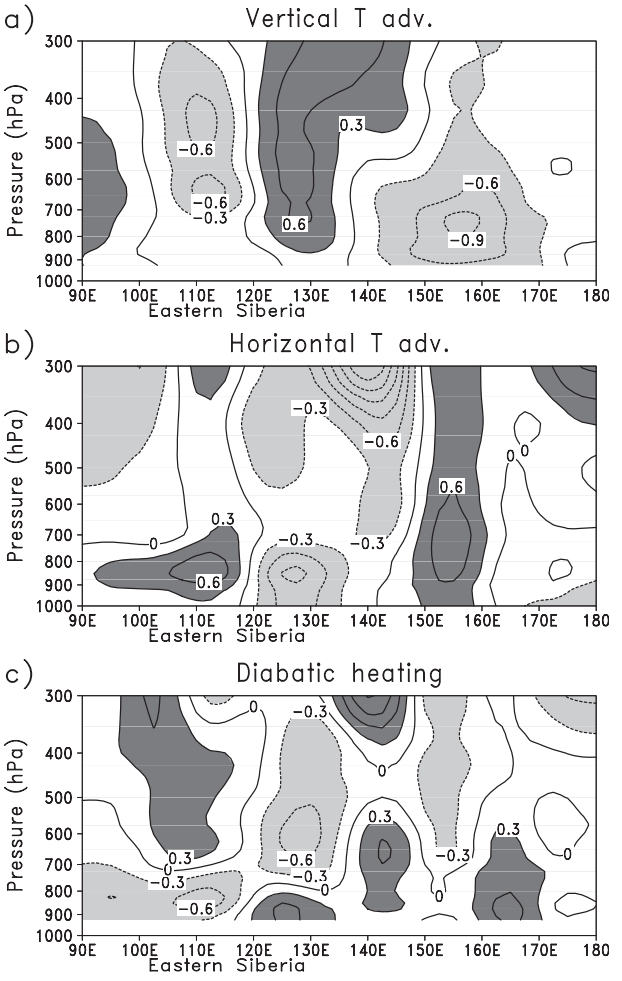

FIG. 8. As in Fig. 6, but for (a) vertical temperature advection ($-\omega\partial\theta/\partial p$), (b) horizontal temperature advection ($-\mathbf{v}\cdot\nabla\theta$), and (c) diabatic heating (Q: residual) differences (K day^{-1}) in the troposphere. Light [dark] shadings represent negative (below −0.3 K day^{-1}) [positive (over 0.3 K day^{-1})] values.

In September Rossby wave activity maintains cyclonic differences over far eastern Siberia (Fig. 9). Although the subpolar jet has disappeared, westerlies tend to strengthen over eastern and far eastern Siberia along 60°N (not shown). Upper-tropospheric anticyclonic differences in eastern Siberia weaken, while in the lower troposphere they are significantly strong (not shown), suggesting a weakening of baroclinic structure. Furthermore, wave activity extends eastward to Alaska and appears to propagate across North America and onward to Europe.

To summarize, enhanced westerlies form a subpolar jet in August. Surface heating over eastern Siberia generates a quasi-stationary Rossby wave that propagates eastward toward eastern Siberia. Rossby wave activity continues throughout September.

c. *East–west dipole in storm track activity*

Figure 10 shows variance differences of 5-day high-pass filtered 300-hPa geopotential height in August and September. In July, storm track activity occurs along the Arctic coast; however, the differences decrease (not shown), suggesting that storm track activity is not substantial for forming the subpolar jet. In August storm track activity weakens in southeastern Siberia and appears to strengthen in southwestern Siberia (although the latter is not statistically significant), resulting in an east–west dipole structure of active differences over southern Siberia. As described by Fukutomi et al. (2004) and MYT, an east–west dipole structure of precipitation differences also occurs over northern Eurasia (Fig. 11). In eastern Siberia, decreased precipitation is a consequence

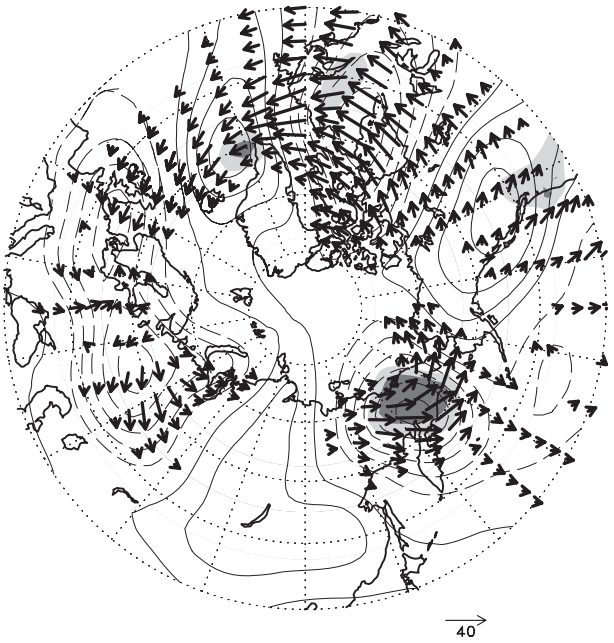

FIG. 9. As in Fig. 5, but for September.

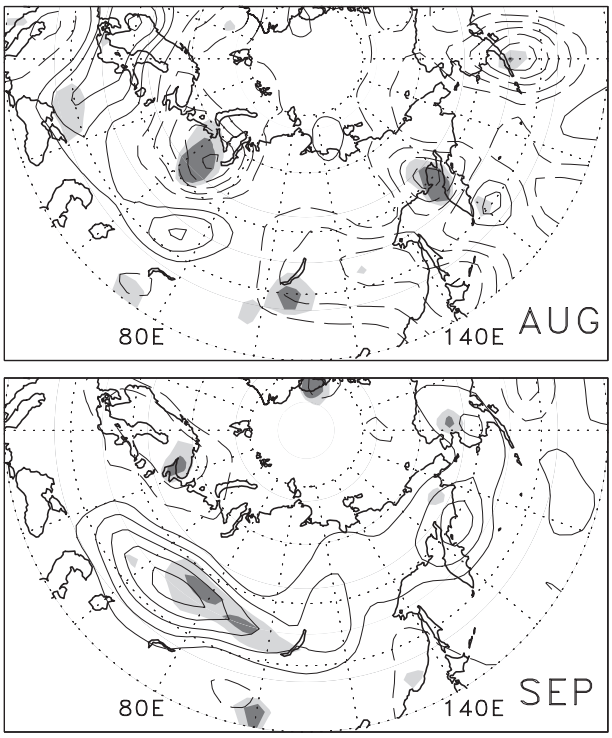

FIG. 10. Variance differences (ESY − LSY) of 5-day high-pass filtered 300-hPa geopotential heights in August (500-m^2 contour interval) and September (1000-m^2 contour interval). Solid contours indicate positive values, and dashed contours indicate negative values. Light (dark) shadings represent differences significant at the 90% (95%) confidence level.

of the snow–hydrological effect, while in southwestern Siberia (at about 60°E), a strengthening of storm track activity appears to contribute to increased precipitation. Storm track activity weakens over Siberia throughout the summer, except in southwestern Siberia.

In September storm track activity differences in southwestern Siberia are significantly stronger than in August, forming an anomalous cyclone to the west and an anomalous anticyclone to the east (Fig. 9). It is possible that anomalous feedback forcing caused by high-frequency transient eddies contributes to amplification and maintenance of the incipient longitudinal dipole structures through anomalous vorticity flux (e.g., Lau and Nath 1991). In far eastern Siberia, the strengthening of storm track activity in September corresponds to strong cyclonic differences.

In general, storm track activity has a feedback effect on the time-mean flow. The feedback effect can be estimated by the vector **E**, using $\mathbf{E} = (\overline{v'^2} - \overline{u'^2}, -\overline{u'v'})$ in which u' and v' are the velocity components of high-frequency transient eddies (Hoskins et al. 1983). The **E** vector is used for a diagnosis for the propagation of transient eddies and their feedback effect onto the time-mean flow. It is approximately proportional to the group velocity of the Rossby wave, and its divergence (convergence) indicates the acceleration (deceleration) of the time-mean zonal wind. Figure 12 shows 2.5-day to 5-day bandpass-filtered **E** vector and div**E** differences in August and September. In August, **E** vectors in western Eurasia converge in a region of strong storm track activity, while **E** vectors extend from east of the Eurasian continent westward, suggesting that anticyclonic differences in eastern Siberia act like a blocking anticyclone. In September, when the anticyclonic differences weaken, eastward **E** vectors extend into eastern Siberia; however, the feedback effect on the time-mean flow is unclear. Consequently, these results suggest that enhanced upstream storm track activity is caused by the time-mean flow as a result

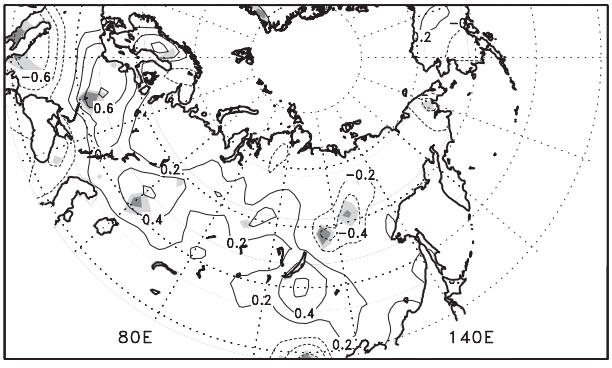

FIG. 11. As in Fig. 3b, but for CMAP precipitation.

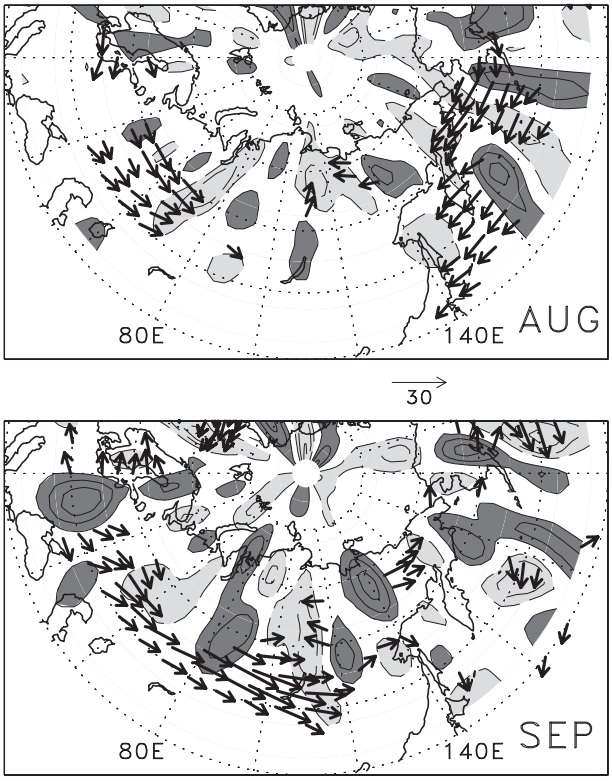

FIG. 12. Bandpass-filtered (2.5–5 days) **E** vector ($m^2\ s^{-2}$) and div**E** (shaded and contours; $1 \times 10^{-5}\ s^{-1}$ contour interval) differences (ESY − LSY) at 300 hPa in August and September. Light [dark] shadings represent negative (below -0.3 K day^{-1}) [positive (over 0.3 K day^{-1})] values.

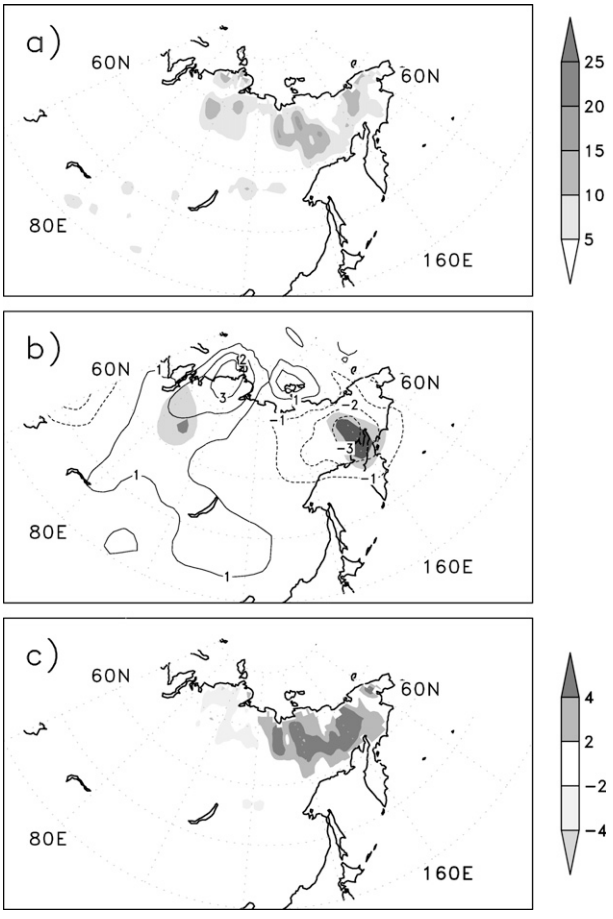

FIG. 13. Surface conditions in September. (a) Mean number of days with snow cover for the period 1988–2004. (b) Surface air temperature differences (ESY − LSY); as in Fig. 3a, but with NCEP reanalysis (2-m air temperature). (c) Difference between the mean number of days with snow cover in ESY and the mean number of days for the period 1988–2004.

of anticyclonic differences in eastern Siberia, resulting in an east–west dipole in storm track activity.

d. Timing of September snow appearance

Far eastern Siberia is the region of earliest snow cover in northern Eurasia (Fig. 13a); by October, snow covers almost all of Siberia. Cyclonic differences over far eastern Siberia (Fig. 9) (with an equivalent barotropic structure from the lower to upper troposphere) result in lower than normal temperatures near the ground surface (Fig. 13b) because of surface northerly differences. In addition, the strengthening of storm track activity (Fig. 10b) results in early snowfall throughout the region (Fig. 13c). These results suggest that early snowmelt in late spring leads to early snow appearance in early autumn over far-eastern Siberia because of summertime land–atmosphere interactions.

5. Possible link to Arctic sea ice response

The Arctic/subarctic climate system depends on a coupling of meteorological conditions in northern Eurasia and the Arctic. In this section, we describe the Arctic sea ice response to anomalous northern snowmelt. Although summer sea ice cover has experienced an accelerated decline since 2005 (e.g., Comiso et al. 2008), we focus on sea ice year-to-year variability prior to the decline. Summer sea ice varies substantially along the Siberian coast in association with year-to-year variations, with decreased cover corresponding to warm temperature anomalies (Ogi and Wallace 2007). Our analysis indicates that surface heating occurs along the Siberian coast in August but not in July (not shown).

Figure 14 (left panels) shows sea level pressure (SLP) differences. Strong anticyclonic differences appear over the Arctic in July and August, forming an equivalent barotropic structure from the lower to upper troposphere (Fig. 5). In July the Siberian coast is on the periphery of strong anticyclonic differences centered over the North

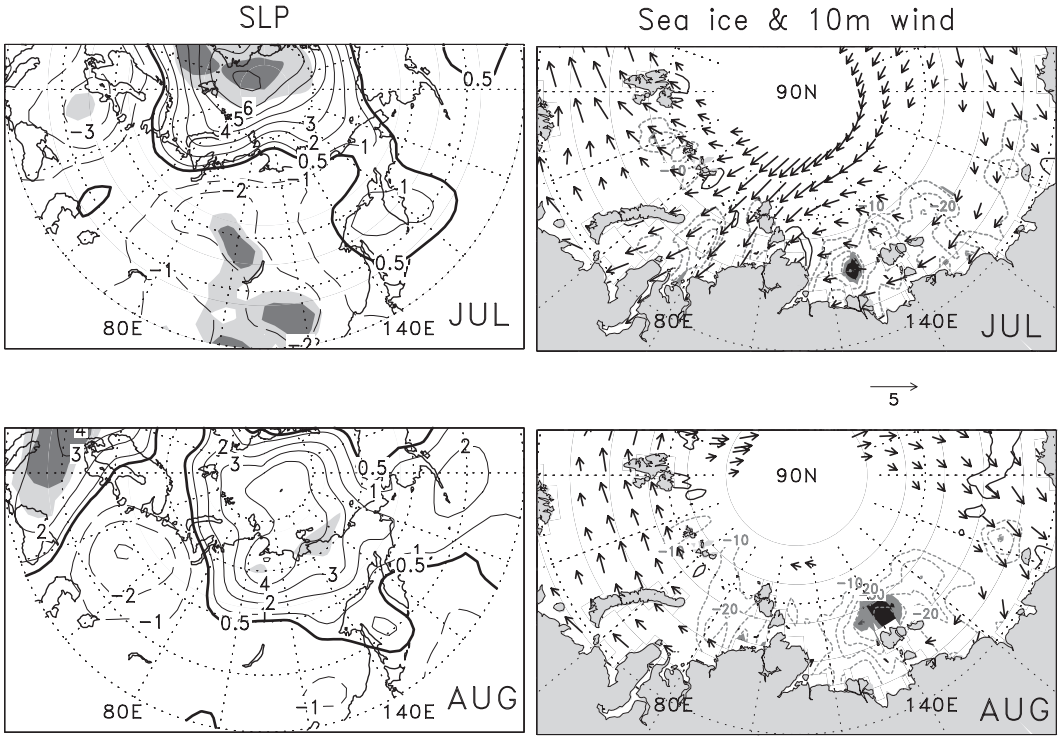

FIG. 14. (left) Sea level pressure (hPa) differences (ESY − LSY) in July and August. Contour interval is 1 hPa, zero contour omitted, and the thick solid contours indicate 0.5 hPa. (right) Sea ice concentration (10% contour interval) and 10-m wind (arrows; m s^{-1}) differences (ESY − LSY). Light (dark) shadings represent differences significant at the 90% (95%) confidence level.

Pole. In August, however, the center of anticyclonic differences is along the Siberian coastline, corresponding to warmer air temperature differences in this region. In contrast, cyclonic differences occur over northern Eurasia in July, except over the Sea of Okhotsk.

Figure 14 (right panels) shows sea ice concentration and 10-m wind differences. Sea ice decreases along the Siberian coast in July, especially in the Laptev Sea, corresponding to easterly wind differences. These results are consistent with those obtained by Ogi and Wallace (2007), who hypothesized that summer circulation anomalies control the sea ice extent, mainly via Ekman drift in marginal seas. In August the sea ice decreases in marginal seas north of eastern Siberia, corresponding to the locus of anticyclonic differences, probably because of increased solar radiation related to decreased cloud cover (absence of wind differences). In September sea ice continues to decrease (not shown), although a relationship with atmospheric variability has not been established. Summer sea ice variability tends to be associated with anticyclonic circulation differences over the Arctic and with easterly wind differences over marginal seas where the year-to-year variability of sea ice concentration is greatest. The present results suggest that variations in northern Eurasian snowmelt result in changes in summertime northern atmospheric circulation and sea ice variability along the coast of Siberia.

6. Summary and discussion

We examined Eurasian subarctic summer climate in response to anomalous snow cover, based on a composite analysis using observational and NCEP reanalysis data. Figure 15 shows a schematic of seasonal changes in ESY from winter to autumn in eastern Siberia, based on the results of MYT and this study. Our analysis confirmed that in ESY—the snow–hydrological effect is active in eastern Siberia and contributes to the formation of the subpolar jet, as reported by MYT.

The soil moisture in the shallow soil layer usually decreases during summer in eastern Siberia after an increase of snowmelt water (Sugimoto et al. 2003). Thus, surface heating due to the snow–hydrological effect may be significant in August. The presence of frozen soil may also influence the snow–hydrological effect. Because of its low conductivity, snow cover may hinder heat transfer between the atmosphere and land surface, thereby influencing a frozen soil layer. It

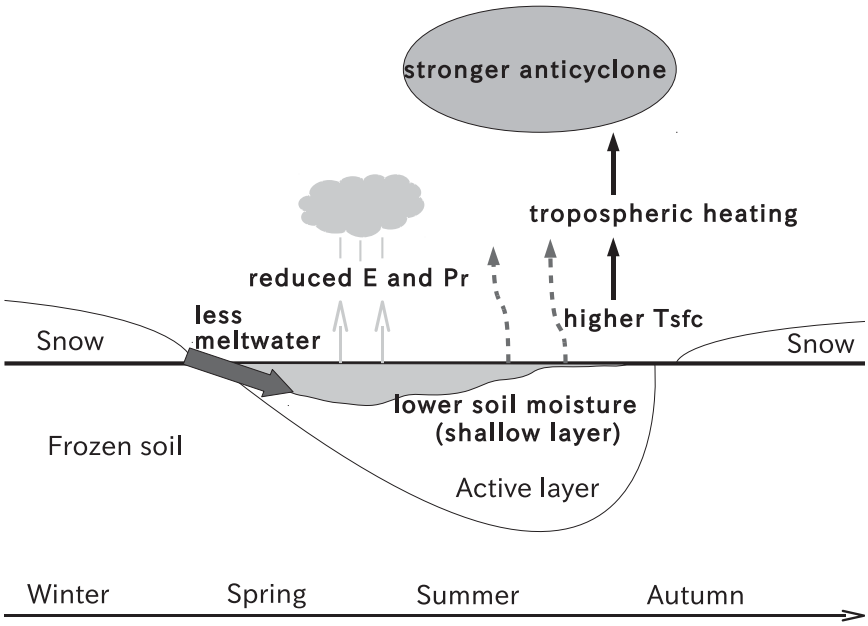

FIG. 15. Schematic diagram of seasonal changes in ESY from winter to autumn in eastern Siberia: E is evaporation, P_r precipitation, and T_{sfc} surface air temperature.

is possible that the snow–hydrological effect as a consequence of the snow cover index in June depends on the surface infiltration of snowmelt water into the soil. Further research is required to better understand the relationship between frozen soil and snow cover on land–atmosphere coupling.

Tropospheric heating over eastern Siberia in August is caused by diabatic heating (condensation heating) associated with ascending air masses and adiabatic heating of descending air masses, as a result of ascending air masses owing to surface heating through the snow–hydrological effect, forming strong anticyclonic differences with a baroclinic structure. In this way, thermal processes related to surface heating generate a stationary Rossby wave that propagates eastward toward eastern Siberia in August. Rossby wave activity is also maintained in September, contributing to the presence of cyclonic differences over far eastern Siberia where the timing of snow is early. The anticyclonic differences in eastern Siberia result in enhanced upstream storm track activity, resulting in an east–west dipole in storm track activity. The snow–hydrological effect may contribute to the amplification and maintenance of baroclinic waves as a consequence of surface heating. In that significant case, the anomalous anticyclone over eastern Siberia appears to act like a blocking anticyclone, as described in this study. MYT showed that a stationary Rossby wave cannot develop in eastern Siberia, although wave activity is faintly visible. However, the MYT experiments were based on a change in the initial snow mass on 1 May, limited to the region north of 60°N; a change in the initial snow mass south of 60°N was not incorporated into the model. For these reasons, the development of the anomalous anticyclone in eastern Siberia might have been suppressed in the MYT model.

As described earlier, the cold regions of the Sea of Okhotsk are bounded in summer by warmer landmasses in far-eastern and eastern Siberia. The frequent occurrence of the Okhotsk high in July and August results in abnormally cool summers because of the cool and wet surface northeasterlies in East Asia. Nakamura and Fukamachi (2004) described the development of the Okhotsk high in early summer in terms of interaction between a stationary Rossby wave packet and surface baroclinicity. On the other hand, in late summer upper-level anticyclonic differences over eastern Siberia (with a ridge extending southeastward) are located to the west of the Sea of Okhotsk, sloping westward with height. The anticyclonic differences with a baroclinic structure may play an important role in the development of the Okhotsk high at the surface in late summer.

According to MYT and the results of the present study, precipitation, accompanied by anticyclonic circulation of moisture flux differences, decreases in eastern Siberia during the summertime. In the JJA mean, cyclonic differences appear over western Eurasia, and anticyclonic differences appear over eastern Eurasia and the Arctic, forming an east–west dipole structure over northern Eurasia (not shown); Fukutomi et al. (2004) reported similar findings based on the 500-hPa geopotential

height field regressed onto the Siberian precipitation seesaw index. Our results further indicate that anticyclonic differences over the Arctic are maintained throughout the summer. In July land–sea gradients of both surface pressure and temperature develop and strengthen across the Arctic coast, possibly resulting in the formation of surface anticyclonic differences over the Arctic. The anticyclonic differences appear to contribute to the year-to-year variability of summer sea ice concentration along the Siberian coast. As far as we know, there is no similar result on the relationship between snowmelt and sea ice variability by either modeling or observational analysis. We can show only the possibility of this link in the present study because of the limitations using statistical analysis. Using an ocean or coupled model may be suitable for further research on this relationship.

In northern Eurasia, the potential predictability due to SST forcing is generally low during all seasons (e.g., Rowell 1998; Matsumura et al. 2010a). For example, errors in land surface state variables, such as soil wetness, can easily degrade climate simulations, especially during summertime (Dirmeyer 2000). Soil moisture and snow cover can act as agents of climate memory at the land surface. Our results suggest that variations in northern Eurasian snow cover and associated land–atmosphere coupling processes have important implications for the predictability of Eurasian subarctic summer climate. Snow cover variations are an important regional forcing factor, contributing to regional land–atmosphere coupling and the development of large-scale atmospheric circulation. A more through understanding of cryospheric and hydrological forcing mechanisms will contribute to the refinement of Arctic/subarctic climate simulations.

Acknowledgments. We thank T. Yasunari and K. Takata for their helpful comments, and three anonymous reviewers for providing useful comments for the improvement of this paper.

REFERENCES

Barnett, T. P., L. Dümenil, U. Schlese, and E. Roeckner, 1989: The effect of Eurasian snow cover on regional and global climate variations. *J. Atmos. Sci.,* **46,** 661–685.

Cohen, J., and D. Entekhabi, 1999: Eurasian snow cover variability and Northern Hemisphere climate predictability. *Geophys. Res. Lett.,* **26,** 345–348.

Comiso, J. C., C. L. Parkinson, R. Gersten, and L. Stock, 2008: Accelerated decline in the Arctic sea ice cover. *Geophys. Res. Lett.,* **35,** L01703, doi:10.1029/2007GL031972.

Dai, A., K. E. Trenberth, and T. R. Karl, 1999: Effects of clouds, soil moisture, precipitation, and water vapor on diurnal temperature range. *J. Climate,* **12,** 2451–2473.

Delworth, T., and S. Manabe, 1989: The influence of soil wetness on near-surface atmospheric variability. *J. Climate,* **2,** 1447–1462.

Dirmeyer, P. A., 2000: Using a global soil wetness dataset to improve seasonal climate simulation. *J. Climate,* **13,** 2900–2922.

Enomoto, T., B. J. Hoskins, and Y. Matsuda, 2003: The formation mechanism of the Bonin high in August. *Quart. J. Roy. Meteor. Soc.,* **129,** 157–178.

Fukutomi, Y., K. Masuda, and T. Yasunari, 2004: Role of storm track activity in the interannual seesaw of summer precipitation over northern Eurasia. *J. Geophys. Res.,* **109,** D02109, doi:10.1029/2003JD003912.

Groisman, P., R. W. Knight, V. N. Razuvaev, O. N. Bulygina, and T. R. Karl, 2006: State of the ground: Climatology and changes during the past 69 years over northern Eurasia for a rarely used measure of snow cover and frozen land. *J. Climate,* **19,** 4933–4955.

Hoskins, B. J., and T. Ambrizzi, 1993: Rossby wave propagation on a realistic longitudinally varying flow. *J. Atmos. Sci.,* **50,** 1661–1671.

——, I. N. James, and G. H. White, 1983: The shape, propagation and mean-flow interaction of large-scale weather systems. *J. Atmos. Sci.,* **40,** 1595–1612.

JMA, 2005: Monthly number of days covered with snow observed by SSM/I. *Monthly Report on Climate System,* No. 11, Japan Meteorological Agency, Toyko, Japan, CD-ROM.

Kanamitsu, M., W. Ebisuzaki, J. Woollen, S.-K. Yang, J. J. Hnilo, M. Fiorino, and G. L. Potter, 2002: NCEP–DOE AMIP-II Reanalysis (R-2). *Bull. Amer. Meteor. Soc.,* **83,** 1631–1643.

Kurita, N., N. Yoshida, G. Inoue, and E. A. Chayanova, 2004: Modern isotope climatology of Russia: A first assessment. *J. Geophys. Res.,* **109,** D03102, doi:10.1029/2003JD003404.

Lau, N. C., and M. J. Nath, 1991: Variability of the baroclinic and barotropic transient eddy forcing associated with monthly changes in the midlatitude storm tracks. *J. Atmos. Sci.,* **48,** 2589–2613.

Matsumura, S., G. Huang, S.-P. Xie, and K. Yamazaki, 2010a: SST-forced and internal variability of the atmosphere in an ensemble GCM simulation. *J. Meteor. Soc. Japan,* **88,** 43–62, doi:10.2151/jmsj.2010-104.

——, K. Yamazaki, and T. Tokioka, 2010b: Summertime land-atmosphere interactions in response to anomalous springtime snow cover in northern Eurasia. *J. Geophys. Res.,* **115,** D20107, doi:10.1029/2009JD012342.

Nakamura, H., and T. Fukamachi, 2004: Evolution and dynamics of summertime blocking over the Far East and the associated surface Okhotsk high. *Quart. J. Roy. Meteor. Soc.,* **130,** 1213–1233.

Ninomiya, K., and H. Mizuno, 1985a: Anomalous cold spell in summer over northeastern Japan caused by northeasterly wind from polar maritime airmass. Part 1: EOF analysis of temperature variation in relation to the large-scale situation causing the cold summer. *J. Meteor. Soc. Japan,* **63,** 845–857.

——, and ——, 1985b: Anomalous cold spell in summer over northeastern Japan caused by northeasterly wind from polar maritime airmass. Part 2: Structure of the northeasterly flow from polar maritime airmass. *J. Meteor. Soc. Japan,* **63,** 858–871.

Numaguti, A., 1999: Origin and recycling processes of precipitating water over the Eurasian continent: Experiments using an atmospheric general circulation model. *J. Geophys. Res.,* **104,** 1957–1972.

Ogi, M., and J. M. Wallace, 2007: Summer minimum Arctic sea ice extent and the associated summer atmospheric circulation. *Geophys. Res. Lett.,* **34,** L12705, doi:10.1029/2007GL029897.

Park, H., T. Yamazaki, K. Yamamoto, and T. Ohta, 2008: Tempo-spatial characteristics of energy budget and evapotranspiration in eastern Siberia. *Agric. For. Meteor.,* **148,** 1990–2005.

Rayner, N. A., D. E. Parker, E. B. Horton, C. K. Folland, L. V. Alexander, D. P. Rowell, E. C. Kent, and A. Kaplan, 2003: Global analyses of sea surface temperature, sea ice, and night marine air temperature since the late nineteenth century. *J. Geophys. Res.,* **108,** 4407, doi:10.1029/2002JD002670.

Rowell, D. P., 1998: Assessing potential seasonal predictability with an ensemble of multidecadal GCM simulations. *J. Climate,* **11,** 109–120.

Shinoda, M., H. Utsugi, and W. Morishima, 2001: Spring snow-disappearance timing and its possible influence on temperature fields over central Eurasia. *J. Meteor. Soc. Japan,* **79,** 37–59.

Sugimoto, A., and Coauthors, 2003: Characteristics of soil moisture in permafrost observed in East Siberian taiga with stable isotopes of water. *Hydrol. Processes,* **17,** 1073–1092.

Suzuki, R., V. N. Razuvaev, O. N. Bulygina, and T. Ohata, cited 2009: Baseline meteorological data in Siberia version 4.1. [Available online at http://www.jamstec.go.jp/iorgc/cgi-bin/database/v01/browse_summary.cgi?program=hcorp&group=CDC&cat=Russia&id=BMDS_41.]

Takaya, K., and H. Nakamura, 2001: A formulation of a phase-independent wave-activity flux for stationary and migratory quasigeostrophic eddies on a zonally varying basic flow. *J. Atmos. Sci.,* **58,** 608–627.

Tibaldi, S., E. Tosi, A. Navarra, and L. Pedulli, 1994: Northern and Southern Hemisphere seasonal variability of blocking frequency and predictability. *Mon. Wea. Rev.,* **122,** 1971–2003.

Watanabe, M., and T. Nitta, 1998: Relative impacts of snow and sea surface temperature anomalies on an extreme phase in the winter atmospheric circulation. *J. Climate,* **11,** 2837–2857.

Xie, P., and P. A. Arkin, 1996: Analyses of global monthly precipitation using gauge observations, satellite estimates, and numerical model predictions. *J. Climate,* **9,** 840–858.

Yasunari, T., A. Kitoh, and T. Tokioka, 1991: Local and remote responses to excessive snow mass over Eurasia appearing in the northern spring and summer climate: A study with the MRI-GCM. *J. Meteor. Soc. Japan,* **69,** 473–487.